J Mater Sci: Mater Electron (2014) 25:4212–4218
DOI 10.1007/s10854-014-2151-4

Synthesis of $Bi_2Fe_4O_9$/reduced graphene oxide composite by one-step hydrothermal method and its high photocatalytic performance

Huajun Sun · Yi Liu · Yong Zhang · Lai Lv · Jing Zhou · Wen Chen

Received: 18 June 2014 / Accepted: 4 July 2014 / Published online: 17 July 2014

Abstract Visible-light-driven degraded organic pollutant with high efficiency is crucial in the current photocatalysis research. A new kind composite photocatalyst with high visible-light photocatalytic activity which consists of $Bi_2Fe_4O_9$ and reduced graphene oxide (RGO) has been synthesized through one-step hydrothermal method at low temperature. Pure $Bi_2Fe_4O_9$ was formed with the addition of graphene oxide (GO) when the concentration of NaOH is 12 mol/L (M) at 180 °C for 72 h hydrothermal reaction. At the same time, the GO was reduced to RGO and adsorbed on the surface of $Bi_2Fe_4O_9$. The resultant composite photocatalyst showed higher absorption not only in the UV range but also in the visible light than pure $Bi_2Fe_4O_9$ indicating more electron–hole pairs generated. The band gap of photocatalysis was reduced from 1.91 to 1.69 eV and recombination of photo-generated electron–hole pairs in composites were decreased through marrying RGO with $Bi_2Fe_4O_9$. As a result, the $Bi_2Fe_4O_9$/RGO composite photocatalyst displayed higher catalytic activity for the degradation of methyl violet under visible light irradiation than rare $Bi_2Fe_4O_9$, promising the use of the $Bi_2Fe_4O_9$/RGO composite in visible-light photocatalysis.

1 Introduction

Photocatalysis is an environmentally friendly method to eliminate organic compounds in wastewater by mineralizing them into the simplest compounds like water and carbon monoxide. In the past decade semiconductor was generally used as photocatalyst to degrade organic dye pollutant [1], which was difficult to be biodegraded [2]. Nowadays, TiO_2, as one kind of metal oxide, has received most attention in this field. However, it exhibits low photocatalytic activity under visible-light irradiation since its activation is limited to UV light due to its wide band gap (3.2 eV). Note that, the energy of UV light makes up only 3–5 % of the solar light and the visible light consisting of 43 % of the solar spectrum [3–5]. As a result, it is highly desirable to develop new materials that are able to respond to visible light irradiation. Among these, bismuth ferrites have great potential as visible-light sensitive photocatalysts due to their narrow band gap [6, 7].

As one kind of bismuth ferrites, mullite-type $Bi_2Fe_4O_9$ is the current research focus as a visible-light active photocatalyst with a band gap of 1.9–2.1 eV [8–10]. Recently, many literatures have reported that $Bi_2Fe_4O_9$ can act as photocatalyst for organic contaminant (methyl orange, methyl red) degradation under visible-light irradiation [11, 12]. However, viewed from reported results up to now, the photocatalytic efficiency of $Bi_2Fe_4O_9$ under visible-light irradiation is not high enough, because the photogenerated electron–hole pairs have a large number of recombination. Therefore, the increasing of the separated electron–hole pair's quantities in $Bi_2Fe_4O_9$ is the key for the enhancement of photocatalytic activity under visible light.

Graphene (GR) is a two-dimensional macromolecular sheet, which possesses many unique properties such as a large specific surface area ($\sim$2630 m^2/g), high mobility of charge carriers (charge-carrier mobility of 250,000 $cm^2 V^{-1} s^{-1}$ at room temperature),good chemical stability and the smallest band gap (0 eV) [13, 14]. Owing to the perfect two-dimension cycle planer structure, graphene can

H. Sun (✉) · Y. Liu · Y. Zhang · L. Lv · J. Zhou · W. Chen
State Key Laboratory of Advanced Technology for Materials Synthesis and Processing, School of Materials Science and Engineering, Wuhan University of Technology, No. 122 Luoshi Road, Wuhan 430070, People's Republic of China
e-mail: huajunsun@whut.edu.cn

function as an excellent catalyst carrier. Ng et al. [15] reported $BiVO_4$/reduced graphene oxide (RGO) composites synthesized under a facile single-step condition and showed remarkable tenfold enhancement in photoelectrochemical water splitting reaction compared with pure $BiVO_4$ under visible illumination. Gao et al. [16] observed that the enhanced photocatalytic activity for the degradation of Rhodamine B (RhB) under visible light contributed to the electronic interaction and charge equilibration between RGO and Bi_2WO_6 which lead to the shift of the Fermi level and decrease the conduction band potential. Sun et al. [17] investigated that $Bi_{25}FeO_{40}$/RGO photocatalyst exhibited higher catalytic activity for the degradation of methylene blue (MB) under visible-light irradiation is due to enhanced MB adsorption and effective suppression of electron–hole recombination via preferential electron transfer from $Bi_{25}FeO_{40}$ to graphene.

Graphene oxide (GO), as one of carbon materials, consists of graphite sheets covalently bonded with oxygen functionalities like hydroxy and epoxide groups on basal planes and carboxyl groups at the edges [18]. The presence of abundant oxygen-containing groups at GO allows interactions with the cations and provides reactive sites for the nucleation and growth of micro-sheets [16]. This characteristic of GO was used in our hydrothermal process, where a facile one-step hydrothermal method was demonstrated to obtain a $Bi_2Fe_4O_9$/RGO composite via hydrothermal reaction in the presence of GO. Because of the unique properties of graphene, it not only improved the separation and transport of photogenerated electrons, but also might cause a smaller band gap indicating a wider range of light absorption [19]. Thus, the $Bi_2Fe_4O_9$/RGO composite photocatalyst exhibited a very higher catalytic activity for degradation methyl violet (MV) under visible light irradiation as compared with bare $Bi_2Fe_4O_9$.

2 Experimental

2.1 Synthesis of the $Bi_2Fe_4O_9$/RGO composite composites

Graphene Oxide (GO) was purchased from Nanjing XFNANO Materials Tech Co., Ltd. $Bi_2Fe_4O_9$/RGO composite photocatalysts were fabricated by a facile one-step hydrothermal method. First, $[Bi(NO_3)_3{\cdot}5H_2O]$ and $[Fe(NO_3)_3{\cdot}9H_2O]$ in a stoichiometric ratio (1 : 1 in molar ratios), as the starting materials, were dissolved in acetone by ultrasonicating and stirring. After dilution by water, concentrated ammonia was dropped in until the pH value of the mixed solution reached 10–11. Then, a required amount of GO dispersions (5 wt%) were added with stirring. The resultant mixture was filtrated and washed by distilled water until the pH value was neutral. Finally, NaOH with different concentrations was added with stirring for 30 min. Subsequently, the solution was transferred to a sealed, Teflon-lined steel autoclave and heated at 180 °C for 72 h. The black powder obtained was washed with distilled water and ethanol through centrifuging and then dried at 70 °C for characterization. For comparison, pure bismuth ferrite without GO was prepared using the same method, which was denoted as $Bi_2Fe_4O_9$ micro-sheets.

2.2 Characterizations

The crystal structures and morphologies of the samples were characterized by X-ray diffraction (XRD, PertPro, PANalytical, Netherlands) and field-emission scanning electron microscope (FESEM, Hitachi S-4800, Japan). To get the microstructural information, Raman spectrum measurements were used on a spectroscopy equipped with a 514 nm laser (Jobinyvon U1000, France). Ultraviolet–Visible diffuse reflectance spectroscopy (UV–Vis-DRS) was performed at room temperature by UV–Visible spectrophotometer (UV-2550). X-ray photoelectron spectra (XPS) were acquired on a VG Mulfilab 2,000 system (Thermoelectron Corporation) equipped with a monochromatized Al-Kα excitation source ($h\nu = 1{,}486.6$ eV). The room temperature photoluminescence spectra were measured on a fluorescence spectrophotometer (RF-5301PC, SHIMADZU) at an excitation of 334 nm.

2.3 Measurements of photocatalytic activity

The photocatalytic activity of $Bi_2Fe_4O_9$/RGO powders were evaluated by the degradation of solution of MV under a 125 W high pressure mercury lamp with a 400 nm cut-off filter as the source of visible-light irradiation with stirring continuously. 30 mg prepared powders were dispersed into 50 mL 30 mg L^{-1} MV solution in a glass beaker. Before being irradiated, each sample was stirred in the dark for 1 h to reach a complete adsorption–desorption equilibrium. At given intervals of irradiation time, 2 mL of the suspension was collected, and the concentration of MV solution was determined by measuring the absorbance with a UV–Vis spectrophotometer. The change of relative absorbance was used to record the change of concentration of MV solution, which was C_t/C_0 (C_t and C_0 referred to the concentration of MV solution at time t and initial time, respectively). All experiments were repeated for six times.

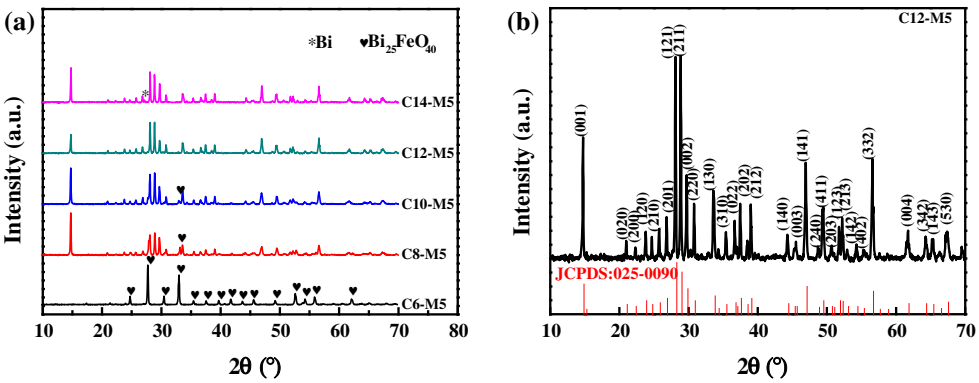

Fig. 1 XRD patterns of **a** as-prepared samples with different concentration of NaOH, **b** as-synthesized $Bi_2Fe_4O_9$-RGO (5 wt%) at 12 mol/L NaOH and PDF No. 025-0090

3 Results and discussion

3.1 Structure and morphology of $Bi_2Fe_4O_9$/RGO composites

The effects of NaOH concentration on the crystallization of bismuth ferrite were investigated. Figure 1a shows XRD patterns of as-prepared samples which were prepared with 5 wt% GO and different concentration of NaOH at 180 °C for 72 h. The samples are named as C6-M5, C8-M5, C10-M5, C12-M5 and C14-M5, according to the concentration of NaOH (M, mol/L) being 6, 8, 10, 12 and 14, respectively. When the concentration of NaOH is below 12 M, mixed phases of a sillenite-type $Bi_{25}FeO_{40}$ with the mullite-type $Bi_2Fe_4O_9$ were observed. Increasing of the concentration of NaOH from 6 to 10 M, the peaks intensity of $Bi_2Fe_4O_9$ is enhanced. At 12 M, all the peaks could be indexed to the pure mullite phase $Bi_2Fe_4O_9$ of the orthorhombic structure (space group: Pbam), which are consistent with the standard data (JCPDS No. 25-0090) showed in Fig. 1b. When the concentration of NaOH exceeds 12 M, impurity of Bi is obtained. According to the literatures [20, 21], the peak at ~11.1° is ascribed to (002) of GO due to the introduction of oxygen containing functional groups attached on both surface and edges of carbon sheets, while the reduction of GO can be confirmed by the appearance of small bumps at ~29° and ~44° due to the removal of a large number of oxygen-containing groups and the formation of much more disordered graphene sheets. For $Bi_2Fe_4O_9$/RGO composite, the disappearance of the GO peak suggests the complete exfoliation of GO due to the insertion of NaOH under hydrothermal process. No diffraction peak of RGO can be observed in the composites, which might be due to the low amount and the extensive exfoliation of RGO. It is obvious that an appropriate alkaline precursor solution is considered favorable for the formation of $Bi_2Fe_4O_9$ when GO exist.

The presence of both $Bi_2Fe_4O_9$ and RGO can be confirmed from the Raman spectra. In the Raman spectra of carbon materials, D band (~1,350 cm^{-1}) associating with the defects of the material and G band (~1,580 cm^{-1}) refers to the presence of sp^2 carbon-type structure that is related to the order of the material, respectively. The ratio of the intensity of D and G bands (I_D/I_G) has been widely used to evaluate the quality of graphene materials coarsely. Meanwhile, it has been reported that G- and D-bands would blue-shifted when GO is reduced to RGO [22, 23]. Figure 2 shows Raman spectra of GO, $Bi_2Fe_4O_9$/RGO composite and pure $Bi_2Fe_4O_9$. In the spectrum of GO, the two characteristic peaks have been observed at 1332 cm^{-1} (D) and 1,590 cm^{-1} (G). In comparison, the G-band shifted from 1,590 to 1,574 cm^{-1}, whereas the D-band shifted from 1,332 to 1,326 cm^{-1} for the $Bi_2Fe_4O_9$/RGO

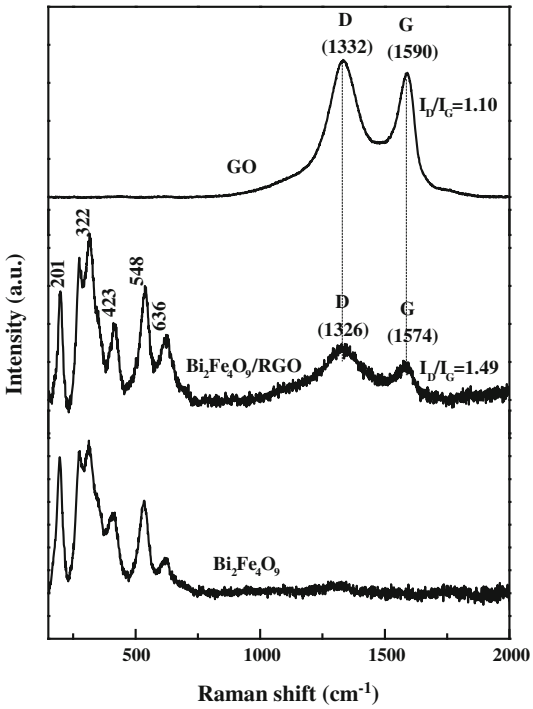

Fig. 2 Raman spectra of GO, $Bi_2Fe_4O_9$/RGO composite and pure $Bi_2Fe_4O_9$

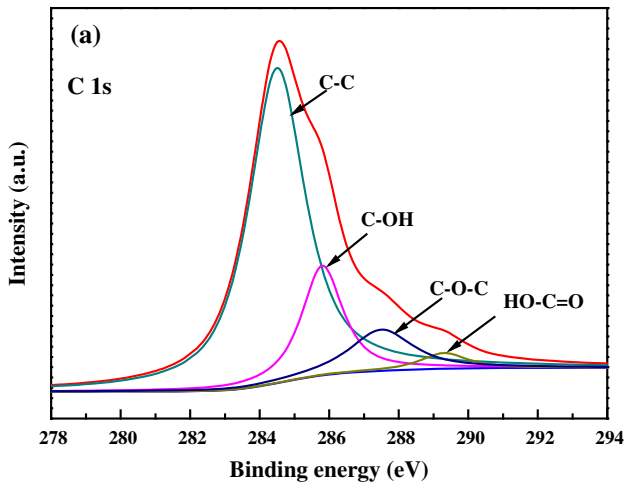

Fig. 3 C1s XPS spectra of $Bi_2Fe_4O_9$/RGO composite

composite. In the meantime, the I_D/I_G ratio of $Bi_2Fe_4O_9$/RGO composite (1.49) increased in comparison with pure GO (1.10), indicating that the disorder ratio of composite has been increased due to a decrease in the average size of the in-plane sp^2 domains upon reduction of the exfoliated GO. This confirms the reduction of GO and presence of RGO in the $Bi_2Fe_4O_9$/RGO composite. The spectra for pure $Bi_2Fe_4O_9$ and $Bi_2Fe_4O_9$/RGO composite display peaks at 201, 322, 423, 548 and 636 cm^{-1} which are consistent to the results reported by Iliev et al. [24] and both Friedrich et al. [25].

XPS can further confirm the reduction of GO in $Bi_2Fe_4O_9$/RGO composite through identifying the oxidation state of C elements. In Fig. 3, the XPS peaks of C1s centered at the binding energies of 289.3, 287.5, 285.8, and 284.5 eV were assigned to the HO–C=O, C–O–C, C–OH, and C=C, respectively. The XPS peak area ratios of the HO–C=O, C–O–C, and C–OH bonds to the C=C bond were calculated and the values are 4.2, 14.4 and 23.6 %. It is obvious that most carbon atoms were sp^2 hybridized, and the amount of oxygen containing functional groups (HO–C=O, C–O–C, and C–OH) on carbon sheets in $Bi_2Fe_4O_9$/RGO was decreased compared with that of GO (the values are 11, 28 and 59 %) [26], indicating that GO in $Bi_2Fe_4O_9$/RGO was reduced to RGO via hydrothermal reaction.

The morphology of $Bi_2Fe_4O_9$, RGO and $Bi_2Fe_4O_9$–RGO composite were observed with SEM as Fig. 4. $Bi_2Fe_4O_9$ exhibited a structure of micro-sheet with the length and width is about 2.0 μm (Fig. 4a). RGO clearly composed of plicated nano-sheets (Fig. 4b). The $Bi_2Fe_4O_9$–RGO composite possessed a mixed morphology of micro-sheets and nano-sheets: the assembling of $Bi_2Fe_4O_9$ micro-sheets on graphene sheets (Fig. 4c), and on the surface of the plates were micro-sheets with the length and width of 1.5 μm (Fig. 4d), which was smaller than that of conventional $Bi_2Fe_4O_9$ micro-sheets (Fig. 4a). This indicates that the introduction of GO in the preparation process of $Bi_2Fe_4O_9$ micro-sheets favors the crystallization of $Bi_2Fe_4O_9$ micro-sheets with smaller sizes.

3.2 Band gap engineering

Figure 5a shows the UV–Vis absorption spectra of $Bi_2Fe_4O_9$ and $Bi_2Fe_4O_9$/RGO composite. The pure $Bi_2Fe_4O_9$ phase exhibited a high absorption in the UV range (200–400 nm) but much low absorption of visible light. The UV and Vis absorption of the $Bi_2Fe_4O_9$/RGO composite both increased when compared with the pure $Bi_2Fe_4O_9$. In such case, more electron–hole pairs can be generated in the $Bi_2Fe_4O_9$/RGO composite using the visible light irradiation. Meanwhile, a red-shift to higher wavelength in the absorption edge of the $Bi_2Fe_4O_9$/RGO composites has also been observed, indicating a narrowing of the band gap of $Bi_2Fe_4O_9$. Shown in Fig. 5b is a comparison between the band gap of pure $Bi_2Fe_4O_9$ microsheets and $Bi_2Fe_4O_9$/RGO composite. It is of significance to note that the band gap is reduced from 1.91 eV to 1.69 eV with the introduction of RGO which was calculated by the Kubelka–Munk method. The band gap narrowing should be attributed to the chemical bonding between $Bi_2Fe_4O_9$ and RGO, that is, the formation of COO–metal bonds, which were also found in the case of TiO_2/graphene [27], CdS/graphene [28], $BiFeO_3$/graphene [29] and $YInO_3$/graphene [30] composites. Because of the increased absorbance, the utilization of solar energy can be more efficient. Therefore, coupling graphene with $Bi_2Fe_4O_9$ is an effective way to improve the photocatalytic activity in visible light.

3.3 Enhanced photocatalytic performance

The photocatalytic activities of pure $Bi_2Fe_4O_9$ and $Bi_2Fe_4O_9$/RGO composite were evaluated by photocatalytic degradation of MV under visible light irradiation. Figure 6 showed the photodegradation rate curves of MV using pure $Bi_2Fe_4O_9$ and $Bi_2Fe_4O_9$/RGO composite as the photocatalyst and the inset is UV–Vis spectra of MV solution after different irradiation time with $Bi_2Fe_4O_9$/RGO composite as the photocatalyst. In the absence of light, MV degradation is only 3.5 %, ruling out that light is an essential element. After 3 h of visible light irradiation, the photo degradation efficiency of MV increases from 19.9 % for pure $Bi_2Fe_4O_9$ to 95 % for $Bi_2Fe_4O_9$/RGO composite.

The degradation kinetics of MB with $Bi_2Fe_4O_9$ and $Bi_2Fe_4O_9$/RGO composite was fitted by the pseudo-first-order kinetics which can be described as the follows:

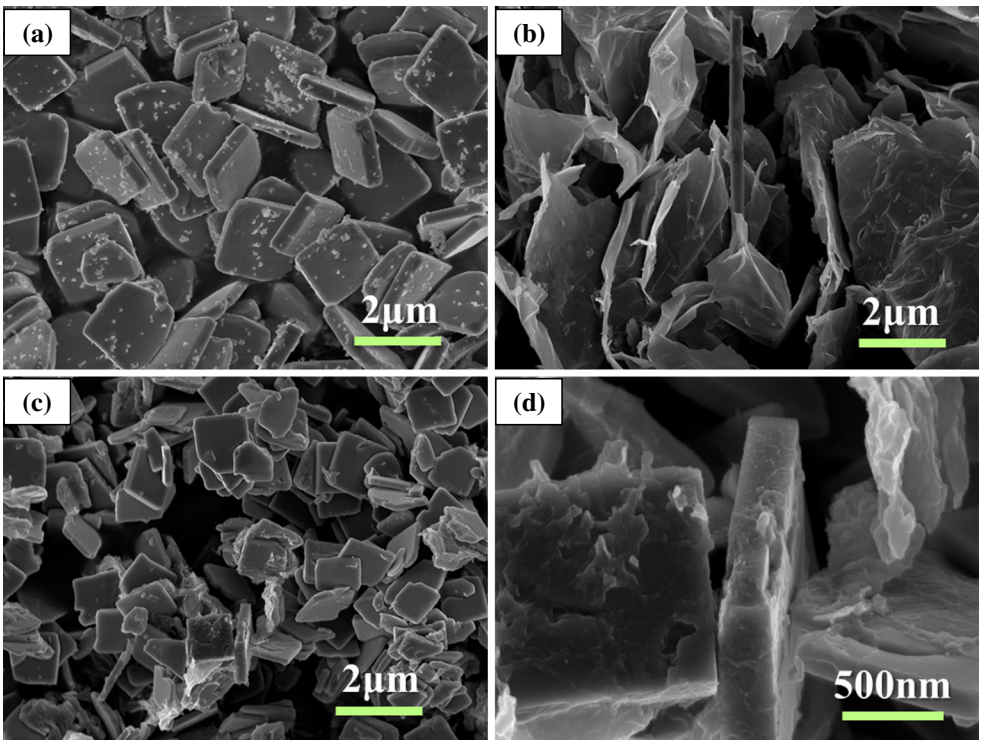

Fig. 4 FESEM images of: **a** $Bi_2Fe_4O_9$ micro-sheets, **b** RGO, and (**c** and **d**) $Bi_2Fe_4O_9$/RGO composite

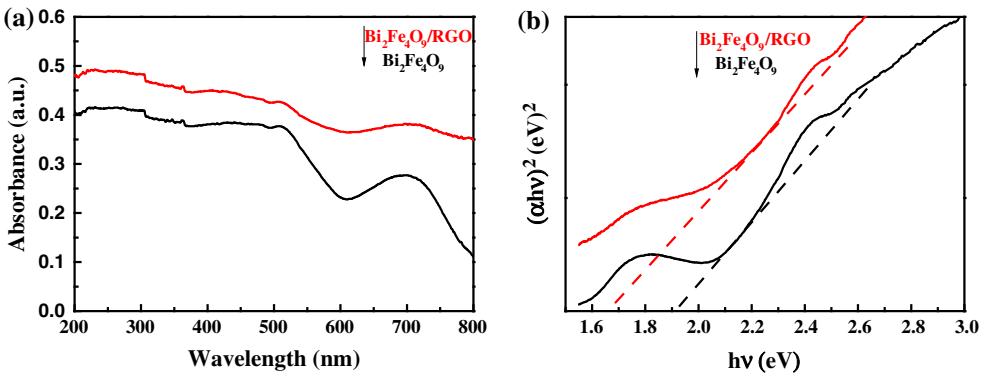

Fig. 5 **a** UV–Vis absorption spectra of $Bi_2Fe_4O_9$ and $Bi_2Fe_4O_9$/RGO composite, **b** the calculated diagrams of their band gaps

$\ln\frac{C_t}{C_0} = K_{obs}t$, where K_{obs} means the observed pseudo-first-order rate constant. The fitting line is plotted in Fig. 7, wherein the slope of the line equals the kinetics rate constant. The K_{obs} of MV removal in the photocatalytic process with $Bi_2Fe_4O_9$/RGO composite was 0.01,639 min^{-1}, which was enormously enhanced compared to that in the process of pure $Bi_2Fe_4O_9$ (0.0012 min^{-1}), showing $Bi_2Fe_4O_9$/RGO composite had better visible light photocatalytic performance. This can be explained by the reduction of Eg and increasing of visible light absorption.

As for a photocatalyst, it is essential to investigate recombination of photo-generated electron–hole pairs for the study of the relevant photocatalytic activity. It is well known, when the electron–hole pairs are induced in the catalyst, they would separate effectively and then transfer to the surface of the catalyst to participate in the redox reaction. However, the recombination of electron–hole pairs would occur in the photocatalyst inner or surface during the transfer process which would lead to a lower photocatalytic activity. In order to confirm the condition about the recombination of induced electron–hole pairs, photoluminescence (PL) spectra were measured for the two samples of pure $Bi_2Fe_4O_9$ and $Bi_2Fe_4O_9$/RGO composite as shown in Fig. 8. The samples exhibited different fluorescence intensity and the emission peak located at the same wavelength of 465 nm. The $Bi_2Fe_4O_9$/RGO composite showed the lower intensity which could be attributed to the less recombination rate of photogenerated electron–hole

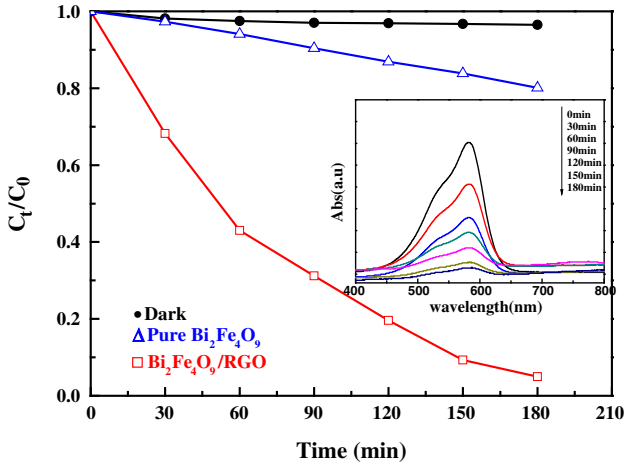

Fig. 6 Photocatalytic degradation of MV using pure $Bi_2Fe_4O_9$ and $Bi_2Fe_4O_9$/RGO composite. The *inset* is the absorption spectra of MV after different irradiation time

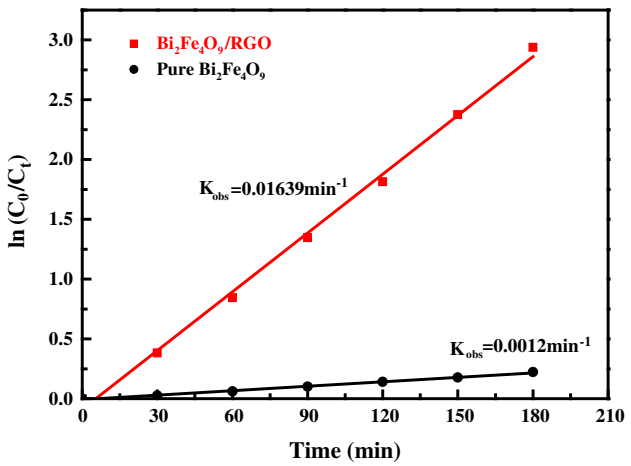

Fig. 7 The kinetics of photocatalytic degradation of MV using pure $Bi_2Fe_4O_9$ and $Bi_2Fe_4O_9$/RGO composite as catalyst

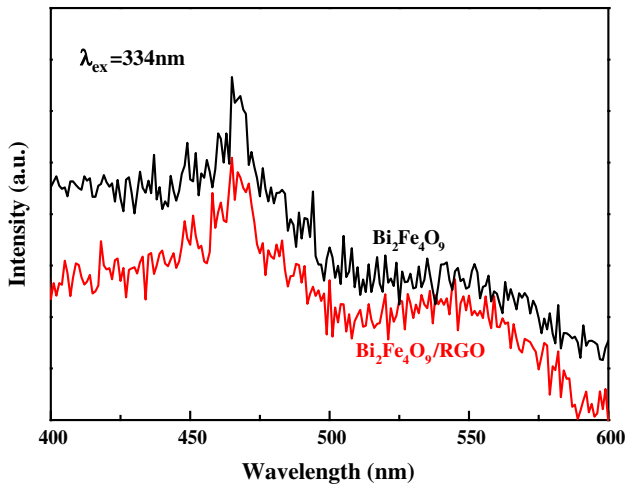

Fig. 8 PL patterns of $Bi_2Fe_4O_9$ and $Bi_2Fe_4O_9$/RGO composite

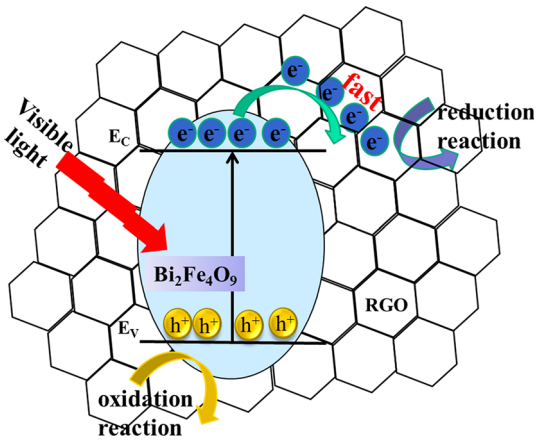

Fig. 9 The catalytic mechanism of $Bi_2Fe_4O_9$/RGO composite under visible light irradiation

pairs. The most likely reason for the less recombination rate of photogenerated electron–hole pairs is the reduced recombination on the catalyst surface. When photogenerated electrons are migrate to the $Bi_2Fe_4O_9$/RGO composite surface, they can be rapidly transferred by the high mobility of photogenerated electrons carriers of RGO which is uniformly distributed on the surface of $Bi_2Fe_4O_9$ micro-sheet.

According to the above results, a probable mechanism for the high photocatalytic degradation activity of $Bi_2Fe_4O_9$/RGO composite is illustrated in Fig. 9. Under visible light irradiation, electrons are excited from the valence band (VB) to the conduction band (CB) of $Bi_2Fe_4O_9$, leaving holes in the VB. The photogenerated electrons rapidly transfer from the CB of $Bi_2Fe_4O_9$ to RGO sheets where they participate in reduction reaction. The holes left on the surface of $Bi_2Fe_4O_9$ oxidize MV to form CO_2, NO_3^- and Cl^- directly. The introduction of RGO in the $Bi_2Fe_4O_9$/RGO composite can reduce the probability of electron–hole recombination, prolonged the lifetime of the charge carriers, and thus enhance the photocatalytic activity. Moreover, the RGO sheets allow the photocatalytic reactions to take place not only on the surfaces of $Bi_2Fe_4O_9$, but also on the RGO sheets with significantly increased reaction sites.

4 Conclusions

In summary, $Bi_2Fe_4O_9$/RGO composite photocatalyst was successfully obtained by one-step hydrothermal method through adjusting the concentration of NaOH at low

temperature in the presence of GO. The GO was reduced to RGO during the hydrothermal process. The photocatalytic activity of $Bi_2Fe_4O_9$/RGO is greatly enhanced compared to rare $Bi_2Fe_4O_9$. Additional, the interface interaction and charge migration between RGO and $Bi_2Fe_4O_9$ lead to the shift of the conduction band and decrease the band gap of $Bi_2Fe_4O_9$/RGO composite, which has a significant influence on photocatalytic process. The enhanced photocatalytic efficiency could be attributed to the reducing band gap of $Bi_2Fe_4O_9$/RGO and fast charge transfer rate, which may be effectively utilized the low energy visible-light and decreasing recombination of the e–h pairs. This work provides an example of one kind of simple one-step hydrothermal synthesis method for preparing graphene-based composite photocatalyst and indicated that $Bi_2Fe_4O_9$/RGO is a very promising candidate for high performance photocatalysts.

Acknowledgments This work was supported from the National Natural Science Foundation of China (Grant Nos. 50802066, 51072145, 51272191 and 51372181) and the Fundamental Research Funds for the Central Universities (Grant No. 2013-IV-034).

References

1. M.R. Hoffmann, S.T. Martin, W.Y. Choi, D.W. Bahnemannt, Chem. Rev. **95**, 69 (1995)
2. I.I. Raffainer, R.P. von Rudolf, Ind. Eng. Chem. Res. **40**, 1083 (2001)
3. B.K. Vijayan, N.M. Dimitrijevic, J.S. Wu, K.A. Gray, J. Phys. Chem. C **114**, 49 (2010)
4. R. Asahi, T. Morikawa, T. Ohwaki, K. Aoki, Y. Taga, Science **293**, 5528 (2001)
5. X. Shu, J. He, D. Chen, Ind. Eng. Chem. Res. **47**, 14 (2008)
6. X. Wang, Y. Lin, X.F. Ding, J.G. Jiang, J. Alloys Compd. **509**, 23 (2011)
7. F. Gao, X.Y. Chen, K.B. Yin, S. Dong, Z.F. Ren, F. Yuan, T. Yu, Z.G. Zou, J.M. Liu, Adv. Mater. **19**, 19 (2007)
8. Q.J. Ruan, W.D. Zhang, J. Phys. Chem. C **113**, 10 (2009)
9. S.S. Qi, R.Z. Zuo, Y. Wang, H.L. Wong, L.W. Chan, J. Mater. Sci. **48**, 11 (2013)
10. S.M. Sun, W.Z. Wang, L. Zhang, M. Shang, J. Phys. Chem. **113**, 29 (2009)
11. T. Tong, D.G. Cai, D.G. Jin, J.R. Cheng, Ferroelectrics **453**, 1 (2013)
12. M. Zhang, H. Yang, T. Xian, Z.Q. Wei, J.L. Jiang, Y.C. Feng, X.Q. Liu, J. Alloys Compd. **509**, 3 (2011)
13. M.J. Allen, V.C. Tung, R.B. Kaner, Chem. Rev. **110**, 132 (2010)
14. G. Williams, B. Seger, P.V. Kamat, ACS Nano **2**, 7 (2008)
15. Y.H. Ng, A. Iwase, A. Kudo, R. Amal, J. Phys. Chem. Lett. **1**, 17 (2010)
16. E.P. Gao, W.Z. Wang, M. Shang, J.H. Xu, Phys. Chem. Chem. Phys. **13**, 7 (2011)
17. A.W. Sun, H. Chen, C.Y. Song, F. Jiang, X. Wang, Y.S. Fu, RSC Adv. **3**, 13 (2013)
18. H. Ying, Z.Y. Wang, Z.D. Guo, D. Zheng, Z.J. Shi, S.F. Yang, Acta Phys. Chimi. Sin. **27**, 6 (2011)
19. X.C. Tao, Q. Hong, T.Z. Xu, F. Liao, J. Mater. Sci. Mater. Electron. (2014). doi:10.1007/s10854-014-2042-8
20. Y. Li, W. Gao, L. Ci, C. Wang, P.M. Ajayan, Carbon **48**, 4 (2010)
21. F.S. Omar, H. Nay Ming, S.M. Hafiz, L.H. Ngee, Int. J. Photoenergy (2014). doi:10.1155/2014/176835
22. Y.S. Fu, X. Wang, Ind. Eng. Chem. Res. **50**, 12 (2011)
23. H. Liu, Y. Su, Z. Chen, Z.T. Jin, Y. Wang, J. Hazard. Mater. **266**, 75–83 (2014)
24. M.N. Iliev, A.P. Litvinchuk, V.G. Hadjiev, Phys. Rev. B **81**, 2 (2010)
25. A. Friedrich, J. Biehler, W. Morgenroth, L. Wiehl, B. Winkler, M. Hanfland, M. Tolkiehn, M. Burianek, M. Mühlberg, J. Phys. Condens. Matter **24**, 14 (2012)
26. Y.S. Fu, X. Wang, Ind. Eng. Chem. Res. **50**, 12 (2011)
27. Y.H. Zhang, Z.R. Tang, X.Z. Fu, Y.J. Xu, ACS Nano **4**, 7303–7314 (2010)
28. N. Zhang, M.Q. Yang, Z.R. Tang, Y.J. Xu, J. Catal. **303**, 60–69 (2013)
29. Z.X. Li, Y. Shen, Y.H. Guan, Y.H. Lin, C.W. Nan, J. Mater. Chem. A **2**, 6 (2014)
30. J.J. Ding, W.H. Yan, W. Xie, S. Sun, J. Bao, C. Gao, Nanoscale **6**, 2299–2306 (2014)